IV International Conference on Particle-based Methods – Fundamentals and Applications
PARTICLES 2015
E. Oñate, M. Bischoff, D.R.J. Owen, P. Wriggers & T. Zohdi (Eds)

DEM PARTICLE CHARACTERIZATION BY ARTIFICIAL NEURAL NETWORKS AND MACROSCOPIC EXPERIMENTS

Luca BENVENUTI [1], Christoph KLOSS [2], Stefan PIRKER [1]

[1] Johannes Kepler University Linz, Department on Particulate Flow Mode lling
Altenbergerstrasse 69, 4040, Linz, Austria
luca.benvenuti@jku.at - www.jku.at/pfm

[3] DCS Computing GmbH
Altenbergerstr. 66a - Science Park, 4040 Linz, Austria
christoph.kloss@dcs-computing.com - www.dcs-computing.com

Key words: Discrete Element Method (DEM) Simulations, Parameter Identification, Artificial Neural Networks

Abstract. The macroscopic simulation results in Discrete Element Method (DEM) simulations are determined by particle-particle contact laws. These usually depend on semi-empirical parameters, difficult to obtain by direct microscopic measurements. Subsequently, macroscopic experiments are performed, and their results need to be linked to the microscopic DEM simulation parameters. Here, a methodology for the identification of DEM simulation parameters by means of macroscopic experiments and dedicated artificial neural networks is presented. We first trained a feed forward artificial neural network by backward propagation reinforcement through the macroscopic results of a series of DEM simulations, each with a set of particle based simulation parameters. Then, we utilized this artificial neural network to forecast the macroscopic ensemble behaviour in dependence of additional sets of particle based simulation parameters. We finally realized a comprehensive database, to connect particle based simulation parameters with a specific macroscopic ensemble output. The trained artificial neural network can predict the behaviour of additional sets of input parameters fast and precisely. Further, the numerical macroscopic behaviour obtained with the neural network is compared with the experimental macroscopic behaviour obtained with calibration experiments. We hence determined the DEM simulation parameters of a specific granular material.

1 Introduction

Particles in various forms - ranging from raw materials to food grains and pharmaceutical powders - play a major role in a variety of industries. Discrete Element Methods ($DEMs$) are widely used to simulate particle behaviour in these granular processes

(Cleary and Sawley [1]).
In their original formulation of DEM, Cundall and Strack [2] allowed two particles to slightly overlap upon contact, and consequently they proposed repulsive forces in relation to this overlap distance. Their fundamental modelling concept has since been widely accepted in the literature and their soft-sphere contact law has been developed further by numerous researchers (Vu-Quoc and Zhang [3] and Di Renzo and Di Maio [4]). With increasing computational resources, DEM simulation have become very popular giving rise to the development of commercial (e.g., $PFC3D$, used by Wensrich and Katterfeld [5]) and open-source software (e.g., $LIGGGHTS$, Kloss et al. [6], Aigner et al. [7]). Soft-sphere DEM simulations of thousands of particles have been proven to faithfully model particle bulk behaviour (Hohner et al. [8]).
In these macroscopic DEM simulations, the contact law kernel between a pair of particles determines the global bulk behaviour of the granular material (Ai et al. [9]). As a consequence, defining a correct contact law is of crucial importance for the predictive capability of DEM simulations. Since DEM contact laws are based on a set of semi-empirical parameters, correct contact law parameters must be defined for a given granular material or DEM simulations will fail (Combarros et al. [10]).
Identifying DEM contact law parameters is not a trivial task. Due to the huge number of particles in a granular material, it may be impractical to identify valid parameter sets by performing bilateral particle collision experiments. Furthermore, some contact law parameters such as the coefficient of rolling friction are purely empirical and cannot be determined by direct particle-to-particle measurements (Wensrich and Katterfeld [5]). Therefore, DEM contact law parameters are commonly determined by comparing the macroscopic outcome of large-scale DEM simulations with bulk experiments (Alenzi et al. [11]). We considered the following parameters: particle radius R (m), size distribution, Young's modulus E (Pa), Poisson's ratio ν (-), time step Δt (s), coefficient of sliding friction μ_s (-), coefficient of rolling friction μ_r (-), coefficient of restitution COR (-), particle density ρ_p (kg/m3), geometry factor $dCylDp$ (-). If DEM simulation results disagree with bulk measurements, the set of contact law parameters must be adjusted until reasonable agreement is achieved.
However, this purely forward methodology of parameter identification is limited by the multi-dimensionality of the parameter space and the associated computational costs of the required DEM test simulations. Moreover, one parameter set which is valid for one bulk behaviour (e.g., angle of repose) might fail for another (e.g., shear tester).
Clearly, there is a need for an efficient method for identifying DEM contact law parameters. In our study, we harnessed Artificial Neural Networks ($ANNs$) in order to reduce the number of DEM test simulations required. $ANNs$ have proven to be a versatile tool in analysing complex, non-linear systems of multi-dimensional input streams (Vaferi et al. [12], and Haykin [13]). In our case, we fed an ANN with DEM contact law parameters as input and compared the output with the bulk behaviour predicted by a corresponding DEM simulation. The difference between ANN prediction and DEM prediction is used

to train our specific ANN with a backward-propagation algorithm (described further below). After a training phase comprising a limited number of DEM test simulations, the ANN can then be used as a stand-alone prediction tool for the bulk behaviour of a granular material in relation to DEM contact law parameters.
In this study, we applied this parameter identification method to two different granular bulk behaviours, namely the angle of repose (AoR) test and the Schulze shear cell (SSC) test. In both cases, we first trained a specific ANN using a number of DEM test simulations before we identified valid sets of DEM contact law parameters by comparing the stand-alone ANN predictions with corresponding bulk experiments. For both cases we obtained valid sets of contact law parameters, which we then compared to formulate a reliable contact law for a given granular material. We further show that the same ANN can be used to characterize different granular materials.
In the next section we define some prerequisites including DEM contact law definitions, a general description of the ANN functionality, and the proposed method of DEM contact law parameter identification. We then describe how it is applied to characterize the DEM contact law parameters of sinter fines.

2 DEM Parameter Identification

Fig. 1 illustrates the methodology used.

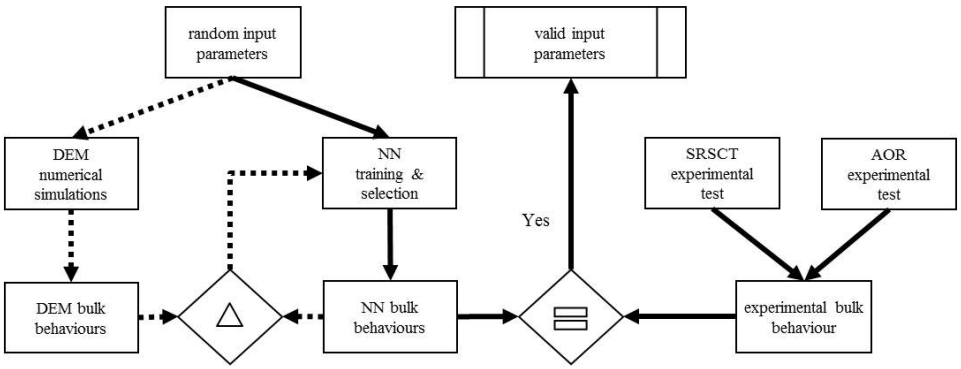

Figure 1: Method. In the training phase (dashed lines) DEM simulations are performed with random initial input parameters. The behaviours obtained are used to train the Artificial Neural Networks ($ANNs$) in a loop that continues until the difference between the outputs of each ANN and its simulations is below the limit (Δ) (see Section 2.2). In the parameters identification phase (solid lines) we identify valid input parameters by comparing ($=$) $ANNs$ and experimental behaviours. Further explanations can be found in Section 2.

2.1 Discrete element method

We decided to utilize a single contact law for all the simulations performed, for details see Benvenuti et al. [18]. The DEM parameters for the Young's modulus (E) and the

Poisson's coefficient (ν) were taken from the literature, see [14] and [15]; however we reduced the former to increase the time step (Δt), following the recommendations of Ai et al. [9]. The time step was between 1.29% and 1.53% of the Rayleigh time, which also depends on the particle density (ρ_p). Furthermore, we locked the size distribution, which was obtained by experimental sieving, see Table 1. In the contact law we used, the tangential component of the contact force between two generic particles (F_t) is truncated to fulfil:

$$F_t \leq \mu_s F_n, \tag{1}$$

where F_n is the normal component and μ_s is the coefficient of sliding friction, one of the particle-based DEM parameter we investigated, another being the coefficient of rolling friction (μ_r). For coarse non-spherical particles, this is a critical parameter and describes inter-particle friction in medium to dense granular flow simulations. It is proportional to the torque counteracting the rotation of the particle. The μ_r parameter enters the equations according to the elasto-rolling resistance model presented by Wensrich and Katterfeld [5] and Ai et al. [9] based on the work of Jiang et al. [16]. The model is called $EPSD2$ in $LIGGGHTS$ and is appropriate for both one-way and cyclical rolling cases. The maximum magnitude of rolling resistance torque is (Eq. 2):

$$T_{r\ max} = \mu_r R_r |\tilde{F}_n| \ , \tag{2}$$

where R_r is the equivalent radius and F_n the normal force. The last two particle-based DEM parameters we investigated were ρ_p and the coefficient of restitution (COR) as defined by Ai. et al. [9]. These coefficients, COR, μ_s, μ_r, ρ_p and $dCylDp$ (the cylinder dimension, proportional to the mean particle diameter), as indicated in Table 2, were constant in each simulation, but their combination differed between simulations. Further, $dCylDp$ was used to evaluate the wall effect, but only 10% of the simulations had a $dCylDp$ larger than 20 (additional information can be found in Benvenuti et al. [18]). The normal stress σ_n and its percentage during the incipient flow condition $\tau_{\%}$ varied to replicate twelve shear-cell load conditions. The complete description of the shear-cell and the AoR simulations can be found in Benvenuti et al. [18]. A Matlab script allowed us to extract from the simulation output the numerical values representative of bulk behaviour (hereafter called *bulk values*) for each DEM simulation parameter combination, which consists of bulk density (ρ_b), coefficient of internal friction in the pre-shear phase (μ_{psh}), coefficient of internal friction in the shear phase (μ_{sh}), and angle of repose (AoR). The first bulk value (ρ_b) was provided directly. For correctly performed simulations, see Benvenuti et al. [18], we observed a stress path as in Fig. 2b. First, the σ_n was kept constant while the coefficient of internal friction (μ_{ie}) initially increased and then reached a plateau. The second bulk value (μ_{psh}) was calculated as the average of the μ_{ie} in this plateau. The σ_n was then automatically reduced, in our example to 80% of its initial value. Subsequently, a second plateau developed. We obtained the third value (μ_{sh}) as the average of μ_{ie} in this second plateau. The stress path accords with the experimental one, especially the

plateaux.
In the AoR tests the average of the repose angles provided us with the fourth bulk value, allowing us to define the numerical bulk behaviour.

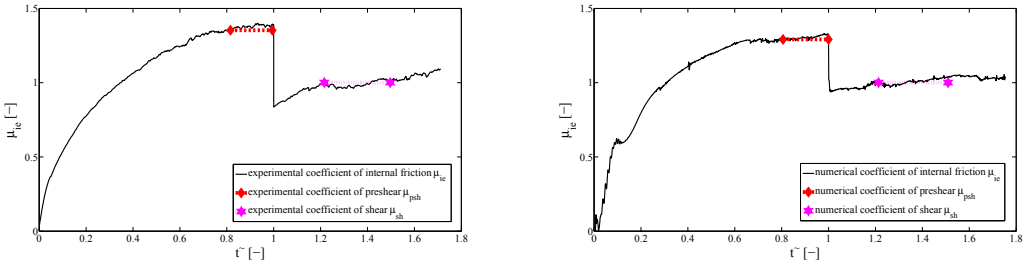

(a) Experimental shear-cell tester stress path - $\sigma_n = 10000\ Pa$

(b) Numerical shear-cell tester stress path - $\sigma_n = 10000\ Pa$

Figure 2: Experimental and numerical samples of the stress path for the Schulze ring shear cell tester. Time was normalized: $\tilde{t} = t/t_{change}$, where t_{change} is the point in time at which the normal stress (σ_n) was modified during the tests. Until $\tilde{t} = 1$, the σ_n was kept constant at 10,000 Pa. In Fig. 2a, a plateau was reached at $\tilde{t} = 0.91$. The coefficient of pre-shear (μ_{psh}) was calculated as the average of the coefficient of internal friction (μ_{ie}) in this first plateau. At $\tilde{t} = 1$, the σ_n was reduced to 80% of its initial value, and soon after a second plateau developed. We obtained the coefficient of shear (μ_{sh}) as the average of μ_{ie} in this second plateau. The stress paths agree well, especially the plateaux. They were clearly relevant because the values representative of the bulk behaviours were collected there.

Mean R (mm)	Std.dev. R (mm)	Young's modulus (MPa)	Poisson's ratio (-)	Δt (s)
0.732	0.41	10	0.40	10^{-6}

Table 1: DEM fixed input values

2.2 Artificial Neural Networks

We first defined the typology of Artificial Neural Networks ($ANNs$) we used and the input we fed them, see Benvenuti et al. [18]. Our $ANNs$ have three different layers: the input layer has a number of neurons equal to the number of different inputs of the network. The hidden (or central) layer's number of neurons was to be investigated. The output layer contains one neuron for the output. The transfer functions between the first two layers are the tangential sigmoid, and those between the hidden and central layers are linear.
Thus, we were able to use the DEM parameter combinations and their corresponding

μ_s (-)	μ_r (-)	COR (-)	ρ_p (kg/m3)	$dCylDp$ (-)
0.4 / 0.6 / 0.8	0.4 / 0.6 / 0.8	0.5 / 0.7 / 0.9	2500 / 3000 / 3500	20 / 36 / 38 / 40

Table 2: DEM variable input values for training the Artificial Neural Networks

	μ_s (-)	μ_r (-)	COR (-)	ρ_p (kg/m3)
range	$[0.1 \dots 1.0]$	$[0.1 \dots 1.0]$	$[0.5 \dots 0.9]$	$[2000 \dots 3500]$
number of values	100	100	25	25

Table 3: DEM random input values. Within each range the indicated number of random values was chosen according to a standard uniform distribution.

bulk values to train the $ANNs$. Note that 15% of the simulations (*test simulations*) were randomly picked and excluded from the training processes. We started with all the DEM parameter combinations and their corresponding numerical μ_{psh} to create 36 $ANNs$ that differed in their numbers of neurons in the hidden layer (between five to forty neurons). We then determined the coefficient of determination (R^2) between the $bulk-macro$ behaviours in the output of the ANN and the 15% *test simulations*, which were not correlated with the remaining 85% used for the training. Thus, we could select for μ_{psh} the ANN with the maximum R^2, again as suggested by Vaferi et al. [12], and we noted its number of neurons. We repeated the same ANN creation steps for μ_{sh}, ρ_b and AoR, obtaining one trained ANN for each bulk value.
Since μ_{psh}, μ_{sh} and ρ_b belonged to the shear-cell simulations, their $ANNs$ were handled together: we had one cluster with three $ANNs$ for the shear cell and one with only one ANN for the AoR. We could then proceed in identifying valid input parameters. Oberkampf et al. [17] suggested using a Design of Experiments (DoE) method to determine the parameter combinations to be simulated. They stated that this approach allows optimization of computation time with an acceptable loss of precision. The speed of the trained $ANNs$ enabled us to follow a different approach to maximizing the precision of the characterization. We created random values in the range and numbers defined in Table 3 according to a standard uniform distribution. The total number of combinations of these random values was 6,250,000. These combinations were then fed to and processed by the selected $ANNs$, and thus three bulk values for the shear cell and one for the AoR were obtained.

2.3 Macroscopic Experiments and Parameter Identification

The experimental characterization was performed as described in Benvenuti et al. [18]. We obtained for each of the twelve load conditions of the SSC three bulk values (μ_{psh}, μ_{sh} and ρ_b). The fourth bulk value was the result of two angle of repose (AoR) tests that recreated the repose angle observed in a pile of the real material.

Subsequently, we compared the ANN and experimental bulk behaviours for the twelve

shear-cell load conditions. If in a DEM-parameter combination all the three bulk values differed by less than 5% from those of the corresponding experiments, i.e.:

$$\begin{cases} \text{if} & |1 - \frac{\mu_{psh,num}}{\mu_{psh,exp}}| < 5\%, \\ \text{and if} & |1 - \frac{\mu_{sh,num}}{\mu_{sh,exp}}| < 5\%, \\ \text{and if} & |1 - \frac{\rho_{p,num}}{\rho_{p,exp}}| < 5\%, \end{cases} \tag{3}$$

the combination was marked. The marked combinations were processed by the AoR ANN, and then compared with the experiment. Were considered valid those that differed by less than 5% also in this comparison (Eq. 4):

$$\text{if} \qquad |1 - \frac{AoR_{num}}{AoR_{exp}}| < 5\%. \tag{4}$$

Further, to prove the validity of the system, we tested the marked combinations by modifying the experimental bulk values of the shear cell. We artificially decreased or increased the shear force, and thus μ_{psh} and μ_{sh}, by a product coefficient (P), e.g. $\mu_{psh,new} = \mu_{psh,old} \cdot P$.

3 Results and discussion

3.1 DEM Simulations

For sinter fine, 546 shear cell and 81 static AoR simulations were run with the parameter combinations described in Table 2. The computational time amounted to 1 hour with 32 AMD cores for a benchmark shear-cell simulation and to 9 hours for a benchmark AoR simulation, both with 50,000 particles. Simulations with larger $dCylDp$ required more time (e.g., about 12 hours for the shear cell with 400,000 particles).

3.2 ANN model development

First, we determined the regression of the bulk behaviour parameters, for instance the μ_{psh}. The plot shows a consistent agreement between the DEM and the ANN values and an almost linear regression ($R^2 = 0.94$). We then investigated how the R^2 changed with the number of neurons for the μ_{psh}. In this case, we achieved a $R^2 = 0.96$ for an ANN with fifteen neurons. Increasing the number of neurons did not improve the R^2; it even started to oscillate with higher numbers of neurons. We subsequently obtained the optimal number of neurons for all $ANNs$. Further, we processed the random combinations (Table 2) with the ANN. The ANN evaluation was significantly faster than the DEM simulations. The individuation of the numerical bulk behaviours for all the DEM combinations did not take more than a few seconds on a single core.

3.3 Experiments and Parameter Identification

Experimental values identifying the bulk behavior, μ_{psh}, μ_{sh} and ρ_b, of sinter fine were acquired through SSC tests. Two AoR tests were performed that gave an average an-

gle of 38.85°. We obtained the radius (R) mean and standard deviations, as shown in Table 1, from sieving experiments. The comparison between numerical and experimental behaviours led to a first series of marked combinations ($MC1$) for one load condition of the shear cell ($\sigma_n = 10,070$ Pa, P=1.0), as plotted in Fig. 3b, where the minimum and maximum values are shown, together with the mean. Note that the confidence interval is large, especially for the COR, which highlights its insignificant influence on the characterization. Both the ρ_p and the μ_s, however, show a narrow confidence interval, which demonstrates their influence and the ability of this procedure to find valid DEM parameters. These results agree with our examination of the ratio of the standard deviation to the range, see Table 4. Further, we observed that various DEM parameter combinations could reproduce the experimental behaviour, and thus evaluated their mutual dependencies. This is shown more clearly in a density plot (see Fig. 4b for $MC1$) of the particles' coefficient of restitution (COR) in relation to the coefficients of sliding friction (μ_s) and rolling friction (μ_r). Multiple combinations (250,407 or 4% of the total) of μ_s and μ_r reproduced the experimental behaviour with varying COR. This underlines once more their correlation, as already stated by Wensrich and Katterfeld [5]. To further demonstrate the validity of the procedure, we modified the product coefficient. First, we set it to $P = 0.8$, and we obtained another series of marked combinations ($MC2$). It can be seen in the parameter space plot in Fig. 3a that the confidence range is narrower than for $P = 1.0$, while in the density plot in Fig. 4a the area appears larger, although slightly less densely populated. Finally, for $P = 1.2$ and its marked combinations ($MC3$) the parameter space plot in Fig. 3c shows a largely different confidence range, while the density plot in Fig. 4c shows a smaller area. As expected, the procedure was highly sensitive to variations in the experimental data. Our approach could therefore be used for a wide range of bulk materials.

We then processed the random combinations with the AoR ANN. In Fig. 5a the parameter space plot for the same criteria as before can be seen. In accordance with theory (Wensrich and Katterfeld [5]), in a simulation dominated by rolling particles, the coefficient of rolling friction has the maximum influence.

Finally, we extracted from the $MC1$ values the AoR ANN behaviour and compared it with the experimental one. As can be seen in the parameter space plot in Fig. 5b, the confidence interval is very small, indicating that all the parameters but the COR played an important role, and demonstrating the reliability of these parameter combinations in representing the bulk behaviour. From the initial 6,250,000 combinations, only 3,884 were valid (0.0621 %), see Table 4.

4 Conclusions

We have presented a two-step method for DEM simulation parameter identification. In the first step, an artificial neural network is trained using dedicated DEM simulations in order to predict bulk behaviours as function of a set of DEM simulation parameters. In the second step, this artificial neural network is then used to predict the bulk behaviour

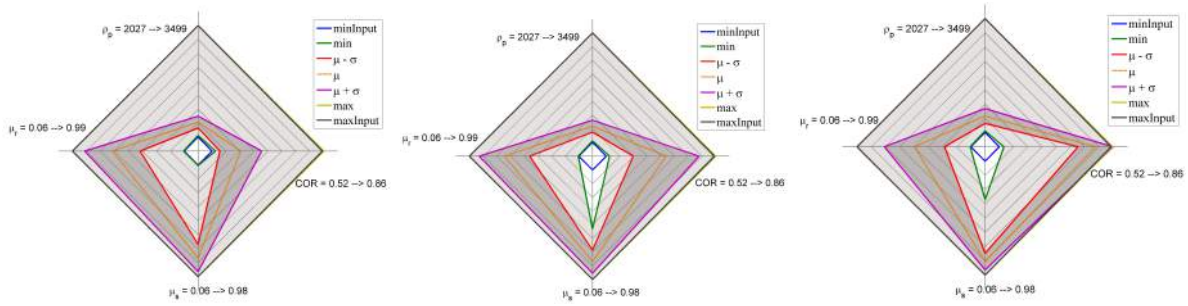

(a) Parameter space plot, SSC, $\sigma_n = 10070$ Pa, P=0.8

(b) Parameter space plot, SSC, $\sigma_n = 10070$ Pa, P=1.0

(c) Parameter space plot, SSC, $\sigma_n = 10070$ Pa, P=1.2

Figure 3: Parameter space plot of valid simulation parameters for three different bulk behaviours measured by a shear cell tester (SSC). Each axis of the parameter space plot represents one simulation parameter. The shaded area indicates valid parameter combinations, and dark shaded values indicate the confidence range. The marked combinations for $\sigma_n = 10070$ Pa are presented. Further explanations can be found in Section 3.3.

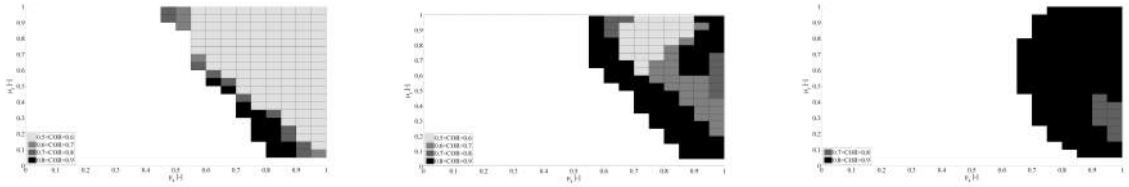

(a) Density plot, SSC, $\sigma_n = 10070$ Pa, P=0.8

(b) Density plot, SSC, $\sigma_n = 10070$ Pa, P=1.0

(c) Density plot, SSC, $\sigma_n = 10070$ Pa, P=1.2

Figure 4: Density plot comparison of shear cell tester (SSC) results. The marked combinations for $\sigma_n = 10070\ Pa$ are presented. Density plot of the particles' coefficient of restitution (COR) as a function of the coefficient of sliding friction (μ_s) and the coefficient of rolling friction (μ_r); in the white area, no valid sets of simulation parameters can be found. In each cell the valid sets are grouped according to the 4 different COR ranges. Each cell is colored according to the group with the most members. The values plotted here were initially selected between the numerical values from the Artificial Neural Network with the original experimental results for the SSC, with a product coefficient $P = 1.0$ (Fig. 4b). Subsequently, they were chosen with a lower virtual shear stress ($P = 0.8$) (4a). The last image (Fig. 4c) represents the selection with a higher virtual shear stress ($P = 1.2$).

	type	SSC	AoR	SSC & AoR
μ_s	mean	0.831	0.177	0.664
$(-)$	std. dev. (SD)	0.097	0.095	0.029
	range (R)	0.9	0.9	0.9
	SD / R	0.108	0.106	0.032
μ_r	mean	0.692	0.830	0.916
$(-)$	std. dev. (SD)	0.215	0.193	0.042
	range (R)	0.9	0.9	0.9
	SD / R	0.239	0.214	0.046
COR	mean	0.708	0.590	0.590
$(-)$	std. dev. (SD)	0.104	0.073	0.065
	range (R)	0.4	0.4	0.4
	SD / R	0.259	0.183	0.161
ρ_p	mean	2245.7	3192.8	2283.9
$(kg/m3)$	std. dev. (SD)	80.5	277.4	67.1
	range (R)	1500	1500	1500
	SD / R	0.054	0.185	0.045
valid	number	290203	816552	3884
combinations	(%)	4.64	13.06	0.06

Table 4: Valid DEM values. For each parameter we show the valid parameter statistics in the two tests and in their intersection. Finally, we show the number of valid parameter combinations over the total (6250000).

of a huge number of additional DEM parameter sets. We can then state that an artificial neural network can be trained by a limited number of dedicated DEM simulations. The trained artificial neural network is then able to predict granular bulk behaviour. Further, this prediction of granular bulk behaviour is much more efficient than computationally expensive DEM simulations. Thus, the macroscopic output associated with a huge number of parameter sets can be studied. If the predictions of the artificial neural network are compared to a bulk experiment, valid sets of DEM simulation parameters can be readily deduced for a specific granular material. More importantly, this DEM parameter identification method can be applied to arbitrary bulk experiments. Combining two artificial neural networks which predict two different bulk behaviours leads to winnowing the set of valid DEM simulation parameters. As part of future work, we will develop this method further by considering different fractions of granular materials, which will lead to size-dependent sets of DEM simulation parameters.

Acknowledgments

This study was funded by the Christian Doppler Forschungsgesellschaft, Siemens VAI Metals Technologies, and Voestalpine Stahl. The authors gratefully aknowledge their support.

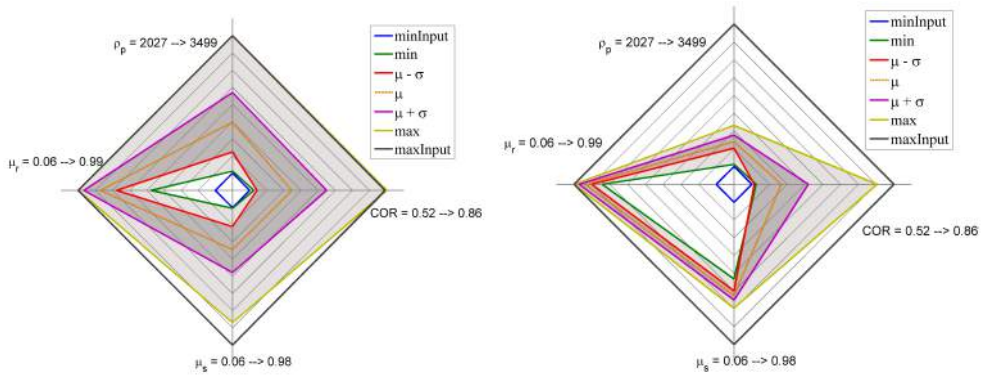

(a) Parameter space plot, $AoR_{exp} = 38.85°$

(b) Parameter space plot, $AoR_{exp} = 38.85°$ & SSC: $\sigma_n = 10070$ Pa

Figure 5: Parameter space plots of valid simulation parameters for the angle of repose tester (AoR) and the combination of AoR and shear cell tester (SSC). Each axis of the parameter space plot represents one simulation parameter. The shaded area and dark shaded values indicate valid parameters combinations and the confidence interval, respectively. Further explanations are given in Section 3.3.

REFERENCES

[1] P. W. Cleary, M. L. Sawley, DEM modelling of industrial granular flows: 3D case studies and the effect of particle shape on hopper discharge, Applied Mathematical Modelling 26 (2) (2002) 89–111.

[2] P. A. Cundall, O. D. L. Strack, A discrete numerical model for granular assemblies, Geotechnique 29 (Volume 29, Issue 1) (1979) 47–65(18).

[3] L. Vu-Quoc, X. Zhang, An accurate and efficient tangential force-displacement model for elastic frictional contact in particle-flow simulations, Mechanics of Materials 31 (4) (1999) 235–269.

[4] A. D. Renzo, F. P. D. Maio, Comparison of contactforce models for the simulation of collisions in DEM-based granular flow codes, Chemical Engineering Science 59 (3) (2004) 525–541.

[5] C. M. Wensrich, A. Katterfeld, Rolling friction as a technique for modelling particle shape in DEM, Powder Technology 217 (0) (2012) 409–417.

[6] C. Kloss, C. Goniva, A. Hager, S. Amberger, S. Pirker, Models, algorithms and validation for opensource DEM and CFDDEM, Progress in Computational Fluid Dynamics, an International Journal 12 (2) (2012) 140–152.

[7] A. Aigner, S. Schneiderbauer, C. Kloss, S. Pirker, Determining the coefficient of friction by shear tester simulation, 3rd International Conference on Particle-Based Methods (2013) 335–342.

[8] D. Hohner, S. Wirtz, V. Scherer, A numerical study on the influence of particle shape on hopper discharge within the polyhedral and multi-sphere discrete element method, Powder Technology 226 (0) (2012) 16–28.

[9] J. Ai, J.-F. Chen, J. M. Rotter, J. Y. Ooi, Assessment of rolling resistance models in discrete element simulations, Powder Technology 206 (3) (2011) 269–282.

[10] M. Combarros, H. J. Feise, H. Zetzener, A. Kwade, Segregation of particulate solids: Experiments and DEM simulations, Particuology 12 (0) (2014) 25–32.

[11] A. Alenzi, M. Marinack, C. F. Higgs, J. J. McCarthy, DEM validation using an annular shear cell, Powder Technology 248 (0) (2013) 131–142.

[12] B. Vaferi, F. Samimi, E. Pakgohar, D. Mowla, Artificial neural network approach for prediction of thermal behavior of nanofluids flowing through circular tubes, Powder Technology 267 (0) (2014) 1–10.

[13] S. Haykin, Neural Networks and Learning Machines, no. v. 10, Prentice Hall, 2009, 2008034079.

[14] N. Tsafnat, N. Amanat, A. S. Jones, Analysis of coke under compressive loading: A combined approach using microcomputed tomography, finite element analysis, and empirical models of porous structures, Fuel 90 (1) (2011) 384–388.

[15] J. Kovacik, Correlation between young modulus and porosity in porous materials, Journal of Material Science 18 (1999) 1007–1010.

[16] M. J. Jiang, H. S. Yu, D. Harris, A novel discrete model for granular material incorporating rolling resistance, Computers and Geotechnics 32 (5) (2005) 340–357.

[17] W. L. Oberkampf, C. J. Roy, Verification and Validation in Scientific Computing, Cambridge University Press, 2010.

[18] L. Benvenuti, C. Kloss, S. Pirker, Identification of dem simulation parameters by artificial neural networks and bulk experiments, manuscript sumbitted for publication.